Journal of Solid State Chemistry 182 (2009) 1211–1216

Contents lists available at ScienceDirect

Journal of Solid State Chemistry

journal homepage: www.elsevier.com/locate/jssc

Some clues about the interphase reaction between ZnO and MnO_2 oxides

F. Rubio-Marcos [a,*], A. Quesada [b,c,d], M.A. García [a,d], M.A. Bañares [e], J.L.G. Fierro [e], M.S. Martín-Gonzalez [f], J.L. Costa-Krämer [f], J.F. Fernández [a]

[a] Instituto de Cerámica y Vidrio, CSIC, 28049 Madrid, Spain
[b] Instituto de Magnetismo Aplicado (ADIF-UCM-CSIC), Madrid, Spain
[c] Insituto de Ciencia de Materiales de Madrid, CSIC, 28049 Madrid, Spain
[d] Departamento de Física de Materiales, UCM, 28040 Madrid, Spain
[e] Instituto de Catálisis y Petroleoquímica, CSIC, Madrid 28049, Spain
[f] Instituto de Microelectrónica de Madrid, CSIC, Tres Cantos, Madrid 28760, Spain

ARTICLE INFO

Article history:
Received 24 October 2008
Received in revised form
9 January 2009
Accepted 6 February 2009
Available online 21 February 2009

Keywords:
$ZnO–MnO_2$ system
Binary oxides
Interphase diffusion
Raman spectroscopy
Magnetic properties

ABSTRACT

Raman spectroscopy is used to evidence both the nature of the interphase reaction between ZnO and MnO_2 particles and its kinetic evolution. Zn cations migrate from the ZnO grains during oxygen vacancies formation process and diffuse into the MnO_2 particles leading to an interphase region with an intermediate valence $Mn^{+3}–O–Mn^{+4}$. Large amounts of desorbed Zn cations promote the formation of $ZnMn_2O_4$ structure, in addition to the intermediate valence state. The system evolves towards complete formation of the spinel phase at higher thermal treatment times. The reactivity of the ZnO plays an important role in the formation of this interphase. Low-reactivity ZnO powder, in which the oxygen vacancies are previously produced, shows a stabilization of the intermediate valence state with very limited formation of the spinel phase. A clear correlation between the amount of the intermediate state interphase and the magnetic properties has been established.

1. Introduction

It has been observed that the interphase created after a partial reaction of two oxides exhibits new and interesting properties due to proximity and diffusion phenomena [1,2] which become relevant at the nanoscale range. An interesting example of these interphase-related properties is the appearance of ferromagnetism after a partial reaction of ZnO and MnO_2 despite the diamagnetic and paramagnetic character at room temperature, respectively, of these oxides [3,4]. After some initial controversy about the origin of this magnetism, which was early ascribed to the formation of a diluted magnetic semiconductor [5], it is clear that this effect appears only after a partial reaction while both initial constituents (ZnO and MnO_2) are present [6,7]. It has been proposed that the magnetism is due to a partial reduction of Mn^{+4} to Mn^{+3} sites, leading to the formation of regions where both oxidation states coexist promoting double exchange [7]. However, no experimental proof of this coexistence has been given and the kinetics of the reaction is still not well described. Therefore, the ultimate origin of this magnetism is still to be elucidated. The nature and structure of the interphase is hard to characterize; X-ray diffraction (XRD) that supplies average structural information fails to point out the presence of interphase reactions and it is not sensitive to the oxidizing states of the ions. This means that if local diffusion had happened it would not be detected by this technique.

In this work, we use Raman spectroscopy as a novel methodology to study the reactivity and the interphases of the $ZnO–MnO_2$ system. Low temperature treatments promote a partial reaction, but not a proper solid solution and sintering (i.e., the situation in which ferromagnetism is experimentally observed); this is used to understand the kinetics of the reaction. X-ray photoelectron spectroscopy (XPS) is also used to determine oxidation states of Mn atoms during the process. With this method, the diffusion of Zn cations into MnO_2 particles is revealed, as well as the coexistence of different manganese oxidation states. Furthermore, we also address how the nature and reactivity of the ZnO powder affects the interphase reaction.

2. Experimental

The compounds with weight nominal composition 2% MnO_2–98% ZnO were prepared following the low-temperature method previously described [3,8]. The compounds were synthesized using two different ZnO's. A first set of compounds was prepared using as raw material commercial ZnO (hereafter, it will be named regular-ZnO), with high purity (>99.99%). In general,

* Corresponding author. Fax: +34 91 735 5843.
E-mail address: frmarcos@icv.csic.es (F. Rubio-Marcos).

0022-4596/$ - see front matter Crown Copyright © 2009 Published by Elsevier Inc. All rights reserved.
doi:10.1016/j.jssc.2009.02.009

low particle size ZnO powders were used because of their higher reactivity. In a second set, the zinc oxide was pre-calcined at 950 °C for 8 h (hereafter, it will be named calcined-ZnO) and the resulting powders were attrition-milled for 3 h. The average particle sizes measured were 0.4, 2.2 and 2.8 μm for regular-ZnO, calcined-ZnO and MnO_2, respectively. The 2% MnO_2–98% ZnO mixtures were homogenized by attrition-milling for 3 h in water. The mixtures were dried overnight and then sieved through a 60 μm nylon mesh. The use of nylon mesh is critical to avoid contamination by cations from standard metallic mesh. These powder samples were annealed in air at 500 °C during different times, ranging from 30 min to 36 h.

Particle size and agglomeration state of calcined-ZnO powder were evaluated by means of a particle size analyzer Malvern Instrument Ltd. Powder morphology was observed by field emission scanning electron microscopy, FE-SEM, Hitachi S-4700.

The Raman scattering was measured in air atmosphere and at room temperature, using 514 nm radiation from an Ar^+ laser excitation line operating at 10 mW. The signal was collected by a microscope Raman spectrometer (Renishaw Micro-Raman System 1000) in the 100–1100 cm^{-1} range.

Photoelectron spectra (XPS) were acquired with a VG ESCALAB 200R spectrometer provided with an Al$K\alpha$ X-ray source (1486.6 eV). Kinetic energies of the photoelectrons of interest were measured using a hemispherical electron analyzer operating in the constant pass energy mode. The base pressure along the analysis was maintained below 5×10^{-9} mbar. Prior to analysis, the samples were cleaned by ion-bombardment with an Ar^+ beam (2 kV) for 2 min. The XPS data were signal-averaged and taken in increments of 0.1 eV with dwell times of 30 ms. Binding energies were calibrated relative to the C1*s* peak from residual carbon contamination of the samples at 284.8 eV. High-resolution spectral envelopes were obtained by curve fitting synthetic peak components using the software package *XPS peak*. Raw data were used with no preliminary smoothing. Symmetric Gaussian–Lorentzian product functions were used to approximate line shapes of the fitting components.

3. Results and discussion

3.1. ZnO samples

Fig. 1 shows the microstructure of the regular ZnO, and calcined ZnO. These micrographs point out an increase in the grain size for the calcined-ZnO and a morphology change. While the regular ZnO shows more prismatic particles, the morphology of the calcined powder corresponds to more spherical particles, with sintering necks. This causes a reduction in the specific surface area and, therefore, a decrease in the active area susceptible to generate interphase reactions.

Fig. 2 shows the Raman spectra for the regular-ZnO and calcined-ZnO samples treated at 950 °C for 8 h. ZnO has a wurzite structure, with two formulae per primitive cell with C_{3v} symmetry. For this structure, the group theory shows that Raman active modes are $A_1+E_1+2E_2$ [9]. These different Raman active modes of ZnO were observed in the spectra. Fig. 2b, shows in detail the A_1(LO) that corresponds to local vibration modes associated with intrinsic lattice defects that may be favored by the crystal growth conditions [10]. This mode is present in both samples and is more intense for calcined-ZnO. The anomalous enhancement of the LO mode has also been reported in doped ZnO [11–13], and ascribed to oxygen vacancies and interstitial Zn.

The Raman spectra were fitted to a sum of Lorenzian lines. The full width at half maximum (FWHM) of the E_2 mode (at 440 cm^{-1}) narrows after the calcination process. The measured FWHM for this mode are 9.4 ± 0.6 and 7.8 ± 0.4 cm^{-1}, for the regular-ZnO and calcined-ZnO, respectively. The narrowing induced by the calcination process is consistent with the increase in grain size [14] during the calcination step, which is evidenced by SEM micrographs.

As a consequence of the calcination steps, two factors affect the reactivity of the ZnO powders (i) the defect generation and (ii) the reduction of the specific surface. The phenomena associated to the generation of defects by the heat treatment in the ZnO powders are related to the loss of oxygen that promotes the formation of $(V_o^+)_s$ defects. The consequent electron availability induces back shift of process and gradual titration of Zn_i^+ defects. During thermal processes in vacuum, desorption of Zn_i^+ and O^{-2} was observed in ZnO powders [15]. Although, the diffusion mechanism of Zn presents controversy, it is established on ZnO single-crystal that zinc diffusivity, in air, may be also controlled by a zinc vacancy mechanism [16].

Therefore, the reactivity of the ZnO powders in presence of another material will be different for both studied powders, regular and calcined powders. For regular ZnO the thermal desorption of Zn_i^+ and the formation of $(V_o^+)_s$ favors the zinc diffusivity in other material and thus promoting the reaction. On the contrary, the reactivity of calcined-ZnO would be smaller because the previous process has already occurred during the calcination step in addition to the surface area reduction.

The Fig. 3a shows the O1*s* core-level spectra with a binding energy of 531.2 eV. The binding energies of various core-levels match well with XPS spectrum of bulk ZnO. The experimental spectra can be fitted to the sum of two components centred at 530.2 and 532.0 eV, which are ascribed to O–Zn–O and to the Zn–OH configuration, respectively. From the fitting, the OH/O ratio was calculated (see Table 1). For regular-ZnO sample, the OH/O ratio (0.31) is larger than for calcined-ZnO (0.26). This is

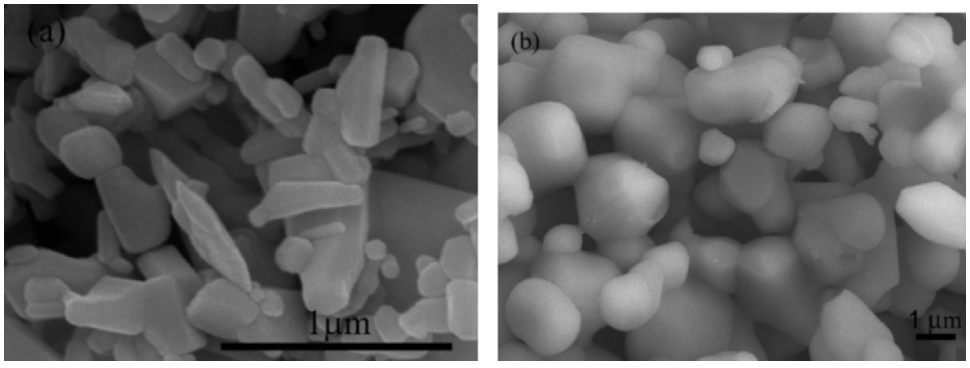

Fig. 1. FE-SEM photographs of the ZnO samples: (a) regular ZnO and (b) calcined ZnO.

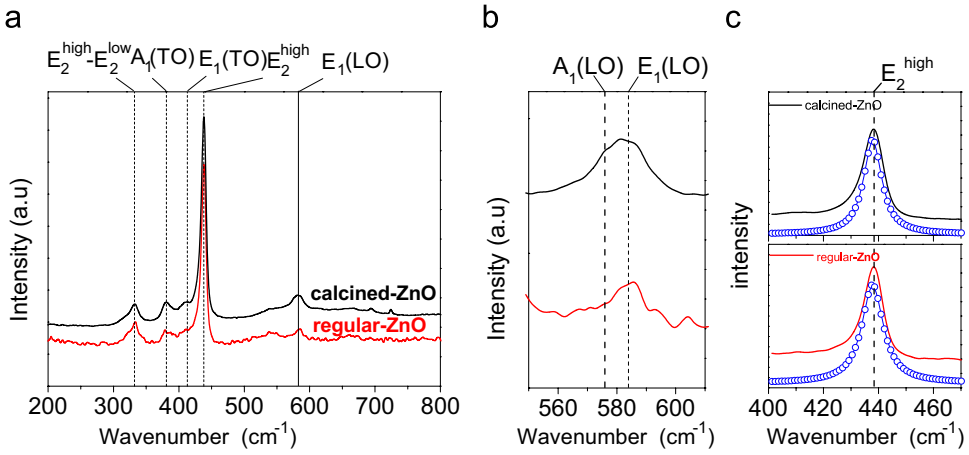

Fig. 2. Raman spectra of the ZnO samples: (a) comparison between the regular-ZnO and the calcined-ZnO, (b) magnified Raman spectra in the ranges of the wavenumber from 550 to 610 cm^{-1} and (c) line shapes of the E_2 mode (at 440 cm^{-1}), were the circles are Lorentzian fits of individual peaks.

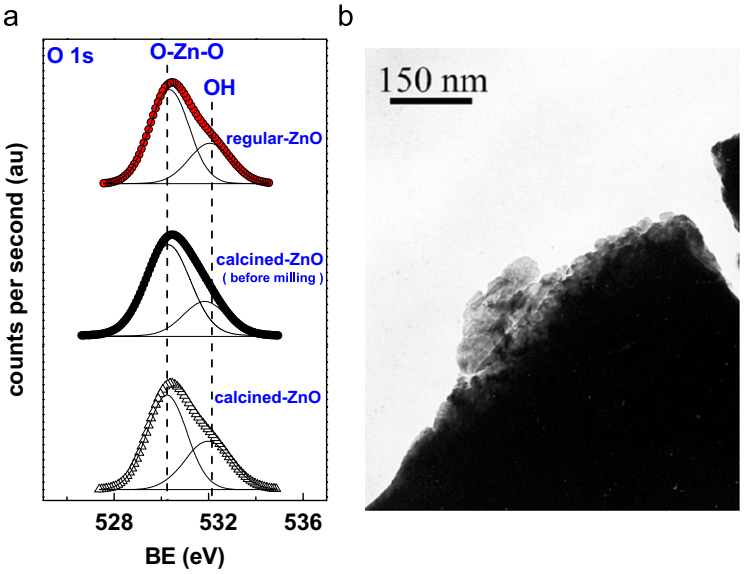

Fig. 3. (a) O1*s* core-level spectra for ZnO samples: regular-ZnO, calcined-ZnO (before milling) and calcined-ZnO and (b) TEM photographs of the calcined-ZnO samples.

Table 1
Binding energies (eV) of core-electrons of ZnO samples; regular-ZnO, calcined-ZnO (before milling) and calcined-ZnO.

Sample	Zn2$p_{3/2}$	O1*s* (%)	OH/O at ratio
Regular-ZnO	1021.7	530.3(69) 532.0(31)	0.31
Calcined-ZnO (before milling)	1021.7	530.2(74) 532.0(26)	0.26
Calcined-ZnO	1021.7	530.2(62) 532.0(38)	0.38

reasonable since OH will be absorbed in the sample surface, and the specific surface area is reduced during calcination. After milling, the calcined-ZnO the OH/O ratio increases up to 0.38 due to the generation of new active surfaces which are able to absorb OH. The TEM micrograph in Fig. 3b confirms the appearance of new reactive surfaces after the milling process.

3.2. *ZnO/MnO_2 samples*

Fig. 4 shows the Raman spectra of the 2% MnO_2–98% ZnO samples, prepared with regular-ZnO and with calcined-ZnO after different times of thermal treatment. In addition to the ZnO peaks, Mn compounds give rise to new peaks located in the range between 600 and 750 cm^{-1} [17]. A detail of this region is presented in Fig. 5, where the spectrum is fitted to the sum of three lorentzian functions centered at 645, 660 and 685 cm^{-1}, and ascribed to MnO_2, MnO_2–Mn_2O_3 and $ZnMn_2O_4$, respectively, according to literature [7,17]. For the samples prepared with regular ZnO the peak at 660 cm^{-1} (MnO_2–Mn_2O_3) dominates after only 30 min treatment, confirming the high reactivity of these samples that favors partial Mn reduction, even at the first stages of the process. Upon longer annealing time, this peak intensity decreases and the peak associated to the spinel ($ZnMnO_4$) at ~681 cm^{-1} emerges concomitantly. Actually, at annealing times as short as 1 h, the formation of the spinel is clearly observed and it becomes more intense than the peak at 660 cm^{-1} after 4 h treatment.

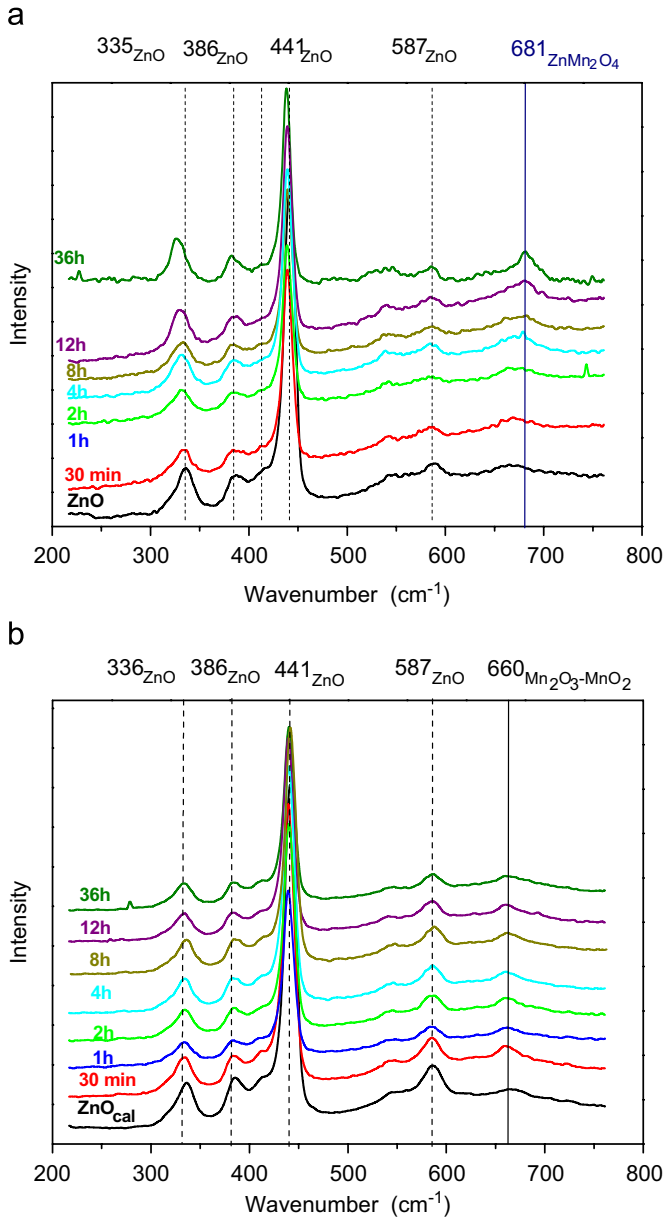

Fig. 4. Raman spectra as a function of the annealing time for (a) 2% MnO_2–98% regular-ZnO and (b) 2% MnO_2–98% calcined-ZnO.

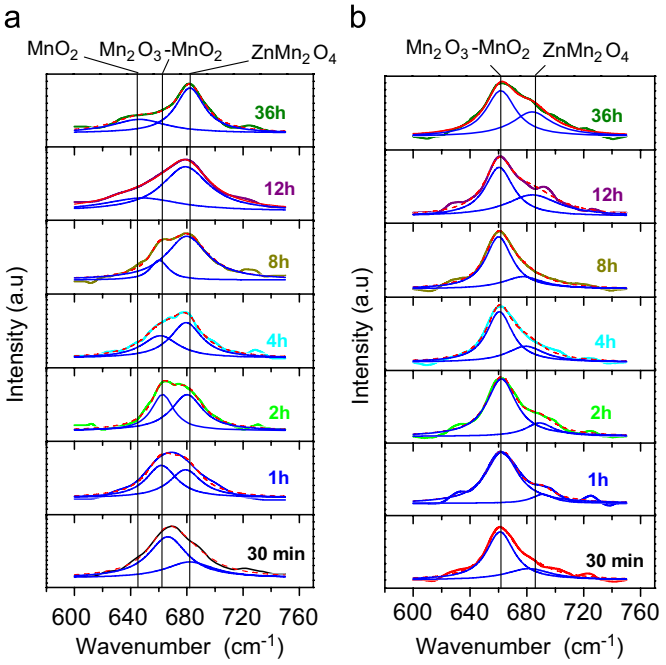

Fig. 5. Magnified Raman spectra in the ranges of the wavenumber from 550 to 610 cm^{-1} as a function of the annealing time and Lorentzian fits of the individual peaks of the Mn compounds region for (a) 2% MnO_2–98% regular-ZnO and (b) 2% MnO_2–98% calcined-ZnO.

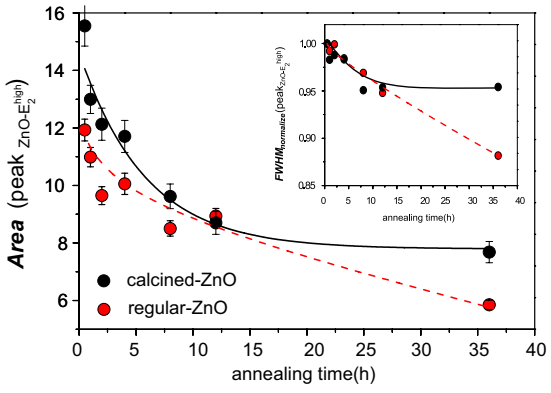

Fig. 6. Decreasing of the E_2^{high} peak area for the 2% MnO_2–98% regular-ZnO and 2% MnO_2–98% calcined-ZnO. The inset shows normalized FWHM of the E_2^{high} peak for the 2% MnO_2–98% ZnO with regular-ZnO and calcined-ZnO.

For the sample prepared with calcined-ZnO, the peak associated to the intermediate species Mn_2O_3–MnO_2 is the most intense at any annealing time, despite the lower reactivity expected after calcination. However, for large annealing times, the formation of the spinel is limited, even after 36 h, and the peak associated to the Mn oxides (660 cm^{-1}) remains dominant. The milling process performed to mix ZnO and MnO_2 creates new reactive surfaces (as evidenced by TEM and XPS) that can favor the initial reduction of manganese sites. Despite this initial high surface reactivity, the previous calcinations process reduced the presence of interstitial Zn_i^+ in the particle. The formation of the spinel requires a large diffusion of Zn atoms (not only those at the particle surface) and therefore is more limited if the samples contains calcined ZnO.

In summary, both regular ZnO and calcined ZnO have an initial high surface reactivity that favors the reduction of $Mn^{+4} \rightarrow Mn^{+3}$, but the reactivity to diffuse Zn atoms to form the spinel phase is much lower in the calcined ZnO; this is due to the reduction of concentration of interstitial Zn_i^+ ions during the calcination step.

In order to perform an in depth analysis of the reaction kinetics, a quantitative analysis of the Raman spectra was done. Peak position, area and width of the E_2^{high} peak were determined from the mathematical fit of the Raman data. The area of the E_2^{high} peak (Fig. 6) exhibits rather different trends, depending on the ZnO used. In general, the E_2^{high} peak area decreases with annealing time. This reduction runs parallel to the decrease in the FWHM values (inset Fig. 6); both parameters have been normalized for comparison purposes. Decreasing FWHM values evidence increasing particle sizes [13]. At short annealing times, $\leqslant$4 h, the area of both samples is essentially the same, confirming a similar initial reactivity due to reactive surfaces. However, these samples exhibit different trends at larger annealing times: the regular ZnO samples exhibit a linear decrease in FWHM values, while these remain stable above 8 h for the samples prepared with calcined ZnO. Furthermore, the total decrease in FWHM is 12–13% for the regular ZnO and only 5% for the calcined ZnO. This result indicates that the amount of Zn capable to react is bigger in regular ZnO. Therefore, the manganese interphase reacts with the Zn generated

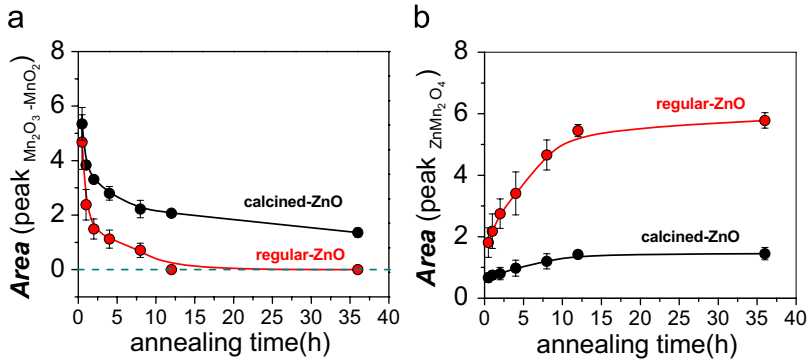

Fig. 7. (a) Decreasing of the Mn_2O_3–MnO_2 peak Area for the 2% MnO_2–98%ZnO with regular-ZnO and calcined-ZnO. (b) Evolution of the $ZnMn_2O_4$ peak area for the 2% MnO_2–98%ZnO with regular-ZnO and calcined-ZnO as a function of the annealing time.

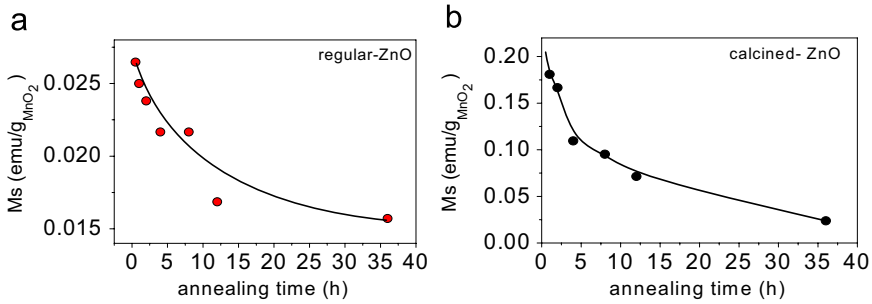

Fig. 8. Evolution of the saturation magnetization with the duration of the 500 °C thermal treatment of the samples made with (a) regular ZnO, and (b) calcined ZnO.

and quickly evolves towards the formation of the spinel phase in regular ZnO. The restricted amount of Zn cations in the calcined ZnO precludes the intermediate state phase.

The analysis of the Raman peaks from Mn is presented in Fig. 7a. The *area* of the peak at 660 cm^{-1} (ascribed to MnO_2/Mn_2O_3) as function of the annealing time, demonstrates again, a trend that depends on the ZnO source. The decrease in the area of the Raman band at 660 cm^{-1} with annealing time is faster for regular-ZnO samples. On the other hand, Fig. 7b shows the annealing time evolution of 681 cm^{-1} peak (ascribed to $ZnMn_2O_4$). A clear correlation between the intermediate manganese state and the spinel phase is derived from Fig. 7a and b. The rapid formation of the spinel consumes the intermediate valence state. As expected, the spinel phase formation is faster for the regular-ZnO samples on the base or more Zn^{2+} cation availability. Actually, the intermediate valence state almost disappears at annealing times longer than 12 h for the regular-ZnO based samples. Surprisingly, at large annealing times, the Raman band associated with MnO_2 appears in the spectrum. This effect could be related to the large presence of spinel restricting the Zn diffusion because of the high cation density of this phase against the manganese ones. Recently, it was reported in this system the formation of the different spinel phases at high temperature [18], which could be related to the differences in Zn cation diffusion.

3.3. Magnetic characterization

The magnetic characterization of as cast MnO_2 and of the $ZnMn_2O_4$ spinel revealed the typical paramagnetic behavior at room temperature (RT), with a magnetic susceptibility of 1.7×10^{-5} emu/(g Oe) for MnO_2 and 2.7×10^{-5} emu/(g Oe) for $ZnMn_2O_4$. This is the expected result since both compounds are antiferromagnetic with Neel temperatures of 84 (MnO_2) and 42 K ($ZnMn_2O_4$). ZnO is diamagnetic with susceptibility $X=-6.4\times10^{-7}$ emu/(g Oe). Magnetization curves were measured for 2% MnO_2–98% regular-ZnO and 2% MnO_2–98% calcined-ZnO samples at room temperature. After the thermal treatments at 500 °C, the two samples showed magnetization curves with a FM signal superimposed to a paramagnetic component as those previously reported [7,16]. Fig. 8 presents the evolution of the saturation magnetization (M_S) as a function of the annealing time for the 2% MnO_2–98% regular-ZnO and 2% MnO_2–98% calcined-ZnO samples. M_S decreases with time similarly to the area of the Mn^{+3}/Mn^{+4} Raman (Fig. 7), underlining a close relationship between the manganese oxidation state and the appearance of magnetism. Larger magnetic signals are found for the calcined ZnO samples. The higher reactivity of regular ZnO may promote a higher availability of Zn cations to diffuse into MnO_2 grains, and thus the stable spinel phase is rapidly formed. Less reactive calcined ZnO renders a slower reaction and therefore the intermediate manganese state persists even for long annealing times, which is claimed to be the origin of this ferromagnetism. A former study determines the absence of room temperature ferromagnetism in the thermally treated MnO_2 that gave a mixture of Mn_2O_3–MnO_2 with the coexistence of Mn^{+3} and Mn^{+4} in the sample [17]. So the mixed valence is required the presence of Zn cations in order to produce room temperature ferromagnetic signal.

4. Conclusions

In summary, Raman spectroscopy proves to be a powerful tool to study the kinetics of the reaction between ZnO and MnO_2. This reaction consists of a diffusion of Zn atoms in the MnO_2 grains to form $ZnMn_2O_4$. The results show that the kinetics of the reaction is determined by the reactivity of the ZnO; it can be limited with a calcination pretreatment. Both regular and calcined ZnO exhibit high initial reactivity due to the highly reactive surfaces created

when milling ZnO and MnO_2. However, subsequent solid-state reactivity is strongly reduced by the calcination pre-treatments; these decrease the concentration of interstitial Zn sites, which are the main source of Zn diffusing atoms into the MnO_2 grains. The magnetic properties associated to the reaction interphase can be controlled by tuning the reactivity of the ZnO.

Acknowledgments

The authors express their thanks to the CICYT Projects MAT2007-66845-C02-01 and FIS2008-06249 and to the MAGIN Project PIF2006-60f0121 for their financial support. F. Rubio-Marcos thanks the FPI-CAM-FSE program for the research grant.

References

[1] A. Brinkman, M. Huijben, M. Van Zalk, J. Huijben, U. Zeitler, J.C. Maan, W.G. Van der Wiel, G. Rijnders, D.H.A. Blank, H. Hilgenkamp, Nat. Mater. 6 (2007) 493–496.
[2] F.Y. Bruno, J. Garcia-Barriocal, M. Torija, A. Rivera, Z. Sefrioui, C. Leighton, C. Leon, J. Santamaria, Appl. Phys. Lett. 92 (2008) 082106.
[3] H. Ohno, Science 281 (1998) 951.
[4] T. Dietl, H. Ohno, F. Matsukura, J. Cibert, D. Ferrand, Science 287 (2000) 1019.
[5] P. Sharma, A. Gupta, K.V. Rao, F.J. Owens, R. Sharma, R. Ahuja, J.M. Osorio Guillen, B. Johansson, G.A. Gehring, Nat. Mater. 2 (2003) 673.
[6] D. Kundaliya, S.B. Ogale, S.E. Lofland, S. Dhar, C.J. Metting, S.R. Shinde, Z. Ma, B. Varughese, K.V. Ramanujachari, L. Salamanca-Riba, T. Venkatesan, Nat. Mater. 3 (2004) 709.
[7] M.A. García, M.L. Ruiz-González, A. Quesada, J.L. Costa-Krämer, J.F. Fernández, S.J. Khatib, A. Wennberg, A.C. Caballero, M.S. Martín-González, M. Villegas, F. Briones, J.M. González-Calbet, A. Hernando, Phys. Rev. Lett. 94 (2005) 217206.
[8] J.L. Costa-Krämer, F. Briones, J.F. Fernandez, A.C. Caballero, M. Villegas, M. Diaz, M.A. García, A. Hernando, Nanotechnology 16 (2005) 214.
[9] C.A. Arguello, D.L. Rousseau, S.P.S. Porto, Phys. Rev. 181 (1969) 1351.
[10] R. Cuscó, E. Alarcón-Lladó, J. Ibáñez, L. Artús, J. Jiménez, B. Wang, M.J. Callahan, Phys. Rev. B 75 (2007) 165202.
[11] J.M. Liu, C.K. Ong, L.C. Lim, Ferroelectrics 231 (1999) 223.
[12] S.K. Sharma, G.J. Exarhos, Solid State Phenom. 55 (1997) 32.
[13] C.L. Du, Z.B. Gu, M.H. Lu, J. Wang, S.T. Zang, J. Zhao, G.X. Cheng, H. Heng, Y.F. Chen, J. Appl. Phys. 99 (2006) 123515.
[14] Y. Du, M.S. Zhang, J. Hong, Y. Shen, Q. Chen, Z. Yin, Appl. Phys. A. 76 (2006) 171–176.
[15] M.G. Cattania, P. d'Antona, F. Morazzoni, R. Scotti, Vacuum 41 (1990) 163–1635.
[16] G.W. Tomlins, J.L. Routbort, T.O. Mason, J. Appl. Phys. 87 (2000) 117.
[17] J.F. Fernández, A.C. Caballero, M. Villegas, S.J. Khatib, M.A. Bañares, J.L.G. Fierro, J.L. Costa-Kramer, E. Lopez-Ponce, M.S. Martin-González, F. Briones, A. Quesada, M. García, A. Hernando, J. Eur. Ceram. Soc. 26 (2006) 3017–3025.
[18] M. Peiteado, S. Sturm, A.C. Caballero, D. Makovec, Acta Mater. 56 (2008) 4028.